Cellulose
https://doi.org/10.1007/s10570-024-06301-0

ORIGINAL RESEARCH

# Apparent specific surface area as an indicator of the degree of cellulose microfibrillation

**Ari Ämmälä · Juho Antti Sirviö · Ossi Laitinen · Henrikki Liimatainen · Ossi Evikari · Sanna Siljander · Tomas Björkqvist**

Received: 19 June 2024 / Accepted: 15 November 2024


**Abstract** Tracking mechanical microfibrillation in nanocellulose production is time-consuming due to a lack of quick characterization methods. This study investigates optical monitoring of the mechanical microfibrillation process by determining the dimensions of microfibrillated cellulose (MFC) particles on micron scale. Bleached hardwood pulp was microfibrillated using three sets of grinding discs in a six-stage pilot process, analyzing MFC characteristics as a function of specific energy consumption via image analysis. A laboratory-scale ultrafine grinder was also used for comparison. The degree of microfibrillation was assessed over a broad energy range using the equivalent diameter derived from the MFC length and width through image processing. The microfibrillation process adhered to Rittinger's law, i.e., changes in the apparent specific surface area (SSA) were linearly proportional to the applied grinding energy. SSA, being inversely proportional to equivalent diameter, predicted MFC quality in terms of nanofilm strength properties. The optical fiber image analyzer proved suitable for online monitoring and control of microfibrillation processes. Despite resolution limits in detecting sub-micron particles, their proportion interrelates to the size of optically visible particles, covering industrial needs for mechanical microfibrillation.

**Keywords** Cellulose nanofibers · Grinding theory · Particle size · Fiber morphology · Mechanical properties · Disc grinder

A. Ämmälä (✉) · J. A. Sirviö · O. Laitinen · H. Liimatainen
Fiber and Particle Engineering, University of Oulu, P.O. Box 4300, 90014 Oulu, Finland
e-mail: ari.ammala@oulu.fi

O. Evikari · S. Siljander · T. Björkqvist
Automation Technology and Mechanical Engineering, Tampere University, PO Box 589, FI-33014 Tampere, Finland

## Introduction

Sustainable materials have gained increasing attention in recent years as society worldwide has awakened to the need for green products and processing technologies. In particular, high-performance materials like cellulose nanofibers (CNFs) or microfibrillated cellulose (MFC) made from renewable biodegradable sources are the center of focus. Various potential applications have been identified for nano and microfibrillated cellulose, for instance in the field of paper and board making (Zambrano et al. 2020), composites (Miao and Hamad 2013), textiles (Felgueiras et al. 2021), food products (Perumal et al. 2022), electronics (Dias et al. 2020), and biomimicking products (Heise et al. 2021). However, production of commercial cellulose nanomaterials remains modest. According to (Miller 2022), in 2022 the annual production capacity of cellulose nanomaterial categorized as mechanically fibrillated MFC with or without

Published online: 08 December 2024

enzymatic or chemical pretreatment, and CNFs prepared primarily through chemical pretreatment was in the order of 21.4 kt and 1.8 kt as dry basis, respectively, while for cellulose filament (CF), a variant of MFC, it totaled 13 kt.

Apart from the high production costs originating from raw material, energy consumption, and possible pretreatment chemicals, one challenge for industrial scale production is the lack of online characterization methods to monitor the quality of CNFs (Balea et al. 2020). In general, characterization of cellulose nanomaterials has been shown to be difficult. Numerous methods for characterizing physical and chemical changes in nanocellulose have been proposed (Varanasi et al. 2013; Kangas et al. 2014; Nair et al. 2014; Foster et al. 2018) including direct morphology analysis using various microscopy techniques such as optical microscopy, scanning electron microscopy (SEM), transmission electron microscopy (TEM), and atomic force microscopy (AFM), as well as indirect methods based on turbidity, transmittance, sedimentation, suspension stability, gel point determination, rheological behavior, and the mechanical properties of nanofiber films. Additionally, the degree of polymerization, assessed through intrinsic viscosity, and crystallization degree have been utilized to evaluate mechanochemical changes.

Despite providing valuable information on nanocellulose properties, many routine characterization methods are laborious and slow, and not suitable for either online use or frequent quality control of cellulose nanomaterials. In turn, image analysis based on optical fiber analyzers is widely used for the online quality measurement of pulp fibers in pulp and paper mills as well as in research laboratories. It has also been used as a complementary method for monitoring the microfibrillation process (Laitinen et al. 2020; Amini et al. 2020; Balea et al. 2021; Zhang et al. 2023). Its usability in routine monitoring and control is still largely unknown, although it has been reported to be used in the monitoring the fineness of microfibrillation in the MFC pilot process (Kumar et al. 2014; Kelly et al. 2021; Zhang et al. 2023), in terms of a sample fines content, which implies the relative proportion of particles shorter than 0.2 mm in length (ISO 16065–2:2014). In addition, attempts have been made to model the mechanical properties of MFC nanofilms based on fiber parameters obtained from image analysis (Pennells et al. 2022).

This study focused on addressing whether the micron-scale dimensional parameters of microfibrillated cellulose obtained from optical image analysis using a state-of-the-art fiber analyzer could be used to monitor a mechanical microfibrillation process. The approach was based on the grinding theory generalized by Hukki (Hukki 1961), which is a widely accepted description of the relationship between applied energy and size reduction. It also serves as a starting point for understanding the mechanisms behind the microfibrillation process. The grinding theory has practical relevance in respect of optimizing the grinding process, development of grinding equipment, and monitoring and controlling the quality and performance of a grinding process online.

The grinding theory suggests that the net grinding energy, $E$, needed for an incremental decrease in particle size $x$ is dependent on the particle size itself, and can be expressed as follows (Hukki 1961):

$$dE = -Kx^{-f(x)}dx, \tag{1}$$

where $K$ is a constant depending on the material properties,

$dx$ is an incremental decrease in particle size $x$, and.

$f(x)$ is an exponent depending on particle size $x$.

Hukki showed that the well-known comminution laws by Rittinger, Kick, and Bond are actually special cases of the generalized form when the exponent $f(x)$ is set as a constant: 2, 1, and 1.5, respectively. In other words, there are distinct narrow operation windows where each law applies when a constant value in the exponent is used.

In respect of microfibrillation, Rittinger's law is the most relevant because it generally addresses fine grinding. Previously, energy consumed in the particle size reduction of wood nanofibers (WNF), measured with a laser diffractometer, was observed to follow Rittinger's law (Ämmälä et al. 2022). By assuming the exponent $f(x)$ to be constant and setting it to 2, as in Eq. 1, after integration it becomes a form that shows that the energy required to reduce the particle size is proportional to the new surface area produced (Wills and Napier-Munn 2015):

$$E = -K'\int_{x_f}^{x_p} x^{-2}dx = K'\left(\frac{1}{x_p} - \frac{1}{x_f}\right), \tag{2}$$

where $x_p$ is the particle size in the product, $x_f$ is the particle size in the feed, and $K'$ is constant for a given raw material and grinding conditions. In microfibrillation, particles are fibrous both in the feed and product, characteristically having a high aspect ratio. As a characteristic particle size to be used in Eq. 2, a volume-based equivalent spherical diameter, $D$, of rod-like particles based on length ($L$) and width ($w$) has been derived by (Jennings and Parslow 1988):

$$D = \left(\frac{3}{2}\right)^{1ex\$1\$/-1ex\$3\$} L\left(\frac{w}{L}\right)^{1ex\$2\$/-1ex\$3\$} = \left(\frac{3L}{2}\right)^{1ex\$1\$/-1ex\$3\$} (w)^{1ex\$2\$/-1ex\$3\$} \tag{3}$$

The specific surface area of particles is defined as their area divided by their mass, which is density, $\rho$, multiplied by volume, $V$. Since an optical measurement detects only particles above sub-micron size, the apparent specific surface area ($SSA$) is introduced here. Using the equivalent diameter of a sphere Eq. (3), and assuming density to be a constant, gives:

$$SSA = \left(\frac{\pi D^2}{\rho 1/6\pi D^3}\right) = \frac{6}{\rho}\left(\frac{1}{D}\right) = kD^{-1} \tag{4}$$

Now, by using the equivalent diameter in the product, $D$, and feed, $D_0$, a change in the specific surface area ($\Delta D^{-1}$) in grinding, Eq. (2) can be expressed as:

$$E = K\left(\frac{1}{D} - \frac{1}{D_0}\right) = K\Delta D^{-1} \tag{5}$$

where constant $K$ combines constants $K'$ from Eq. (2) and $k$ from Eq. (4).

In this study, we hypothesized that the progress of the microfibrillation process (degree of microfibrillation) with disc grinders is directly correlated to the equivalent diameter of the MFC particles measured with an advanced optical fiber analyzer. Although the wavelength of the light limits the resolution of image analysis, the accumulation of small, optically invisible material during grinding correlates with a reduction in the size of the particles being optically measured, suggesting that the measured particle size reflects changes in the overall particle size distribution.

The apparent specific surface area was expected to be linked to the mechanical properties of MFC nanofilms. Since SSA is inversely proportional to particle size, an increasing degree of microfibrillation resulting in smaller particle size is anticipated to provide a larger bonding area for nanofilms. A smaller particle size also enables tighter packaging of particles during film formation, whereas a large surface area promotes hydrogen bonding, thereby contributing to the consolidation of the film structure.

## Materials and methods

### Pulp

Two batches of dried, bleached birch kraft pulp from Finnish pulp mills were selected for the study. One was pre-refined to a freeness (CSF) of 250 mL using a conical disc refiner (Valmet RF01) at a consistency of 4.5%, with a specific energy consumption of 100 kWh/t (net) and a specific edge load of 0.4 J/m. After refining, the length-weighted fiber length (ISO 16065–2:2014) was 0.82 mm, and the width was 10.3 µm. The other pulp, used in lab-scale grinding, had a length-weighted fiber length (ISO 16065–2:2014) of 0.93 mm and a width of 16.9 µm.

### Microfibrillation

Pre-refined pulp was microfibrillated with a pilot grinder (in-house design by Tampere University) using three different sets of mineral-coated disc design after fiber cutting pre-refining. In the first series (denoted as Pilot1) discs with a fine surface texture were employed while in the second series (Pilot2) a coarse surface texture was used. In the third test series (Pilot3) the same surface texture was used as in the first series, but the inlet design was modified. Each series was performed at a consistency of 2% and the pulp underwent six cycles through the grinder, each time with a smaller disc gap while keeping the disc rotation frequency constant. Total power consumption during microfibrillation was recorded from an inverter (Vacon, Finland). In the calculation of the specific energy consumption (SEC) no-load power was subtracted from the total power consumption. Samples were collected after each pass for particle size analyses and for the preparation of MFC nanofilms.

Pulp without pre-refining was microfibrillated using a laboratory-scale Masuko MKCA6-2J (Masuko Sangyo, Japan) ultra-fine grinder. Laboratory grinding (denoted as Lab Ref) was conducted at a

consistency of 1.5% with a rotor speed of 1500 rpm. Eleven passes were employed while gradually tightening the disc gap from 0 to −100 µm. Samples were extracted for analysis after each pass. Power consumption was measured with an energy meter (iEM3250 Schneider-Electric, France). Similarly to the pilot experiments, no-load power was subtracted from the total power consumption.

Analysis of MFC dimensions by image analysis

The dimensions of MFC particles were analyzed with a FS5 Fiber Image Analyzer (Valmet Automation, Finland), which employs an ultra-high density (UDH) camera and automated advanced image processing to characterize MFC particles. A dilute MFC sample is pumped through a cuvette, and the analyzer records over 3000 images from which particle dimensions are analyzed. The spatial resolution of the method is on the order of 1 µm (Laitinen et al. 2020). An example of a processed image having a size of 16.2 × 13.5 mm is presented in Fig. 1. The number of visible particles varied in between one million to tens of millions depending on the degree of microfibrillation and sample consistency.

The samples were diluted to 0.67 g/L and, due to visually observable flocs, dispersed with an Ultra-Turrax unit (IKA T25, Germany) at 12000 rpm for 1 min. After dispersing, the suspension was further diluted to 0.02 g/L, and a volume of 200–250 mL was dosed for the measurements. During the

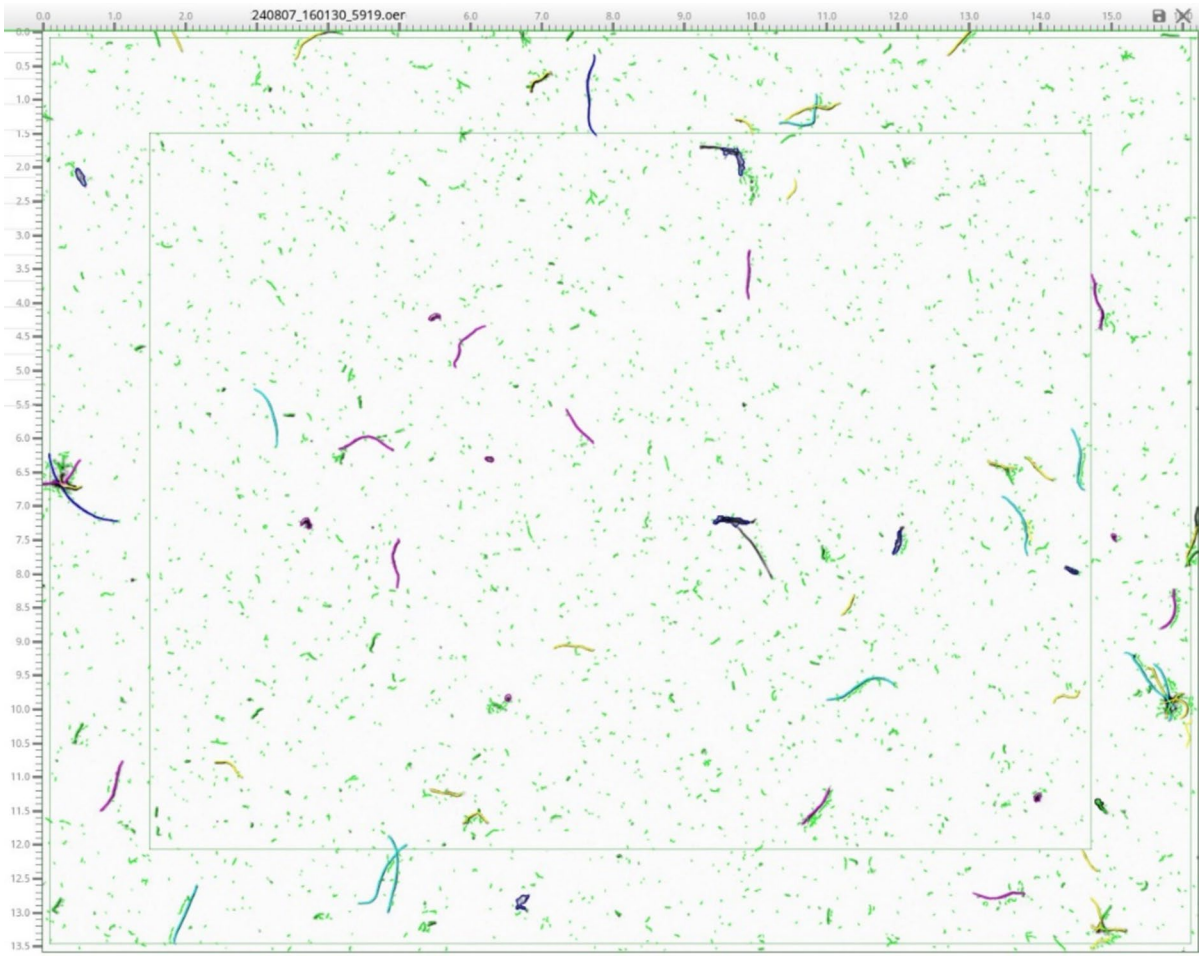


**Fig. 1** Example of a processed image of MFC (Pilot2 after 5th pass) with the FS5 analyzer

analysis, the device automatically fine-tuned the consistency according to its internal specifications.

The length-weighted fiber length and width obtained from the image analysis were used in calculating the equivalent diameter (Eq. 3).

### Nanofiber content by centrifugation method

The nanofiber content was determined in two replicate samples by dispersing them with the Ultra-Turrax device for 1 min at 12 000 rpm, followed by centrifugation (Beckman Coulter Avanti J-26 XPI, USA) in a dilute suspension of 2 g/L at 1254 G (Serra-Paradera et al. 2021). The supernatant, containing the small particle fraction, was carefully decanted, dried at 103 °C, and weighed ($m_{sup}$). The sediment, containing the larger particles, was also dried and weighed ($m_{sed}$), and the nanofiber proportion ($x_{nano}$) was calculated as

$$x_{nano} = \frac{m_{sup}}{m_{sup} + m_{sed}} 100\% \tag{6}$$

### Mechanical properties

Nanofilms (grammage of 66 ± 4 g/m$^2$) were prepared from the MFC samples by filtration in a dilute suspension (2 g/L), which was dispersed beforehand with the UltraTurrax device at 12000 rpm for 1 min, on a membrane (Durapore) with a pore size of 0.65 µm. The films were dried with a Rapid-Köthen sheet dryer (Karl Schröder KG, Germany) at 93 °C using a vacuum of 0.1 bar (ISO 5269–2:2004). Before any measurements were taken, the films were conditioned at 23 °C at a relative humidity of 50%.

The thickness of the films was determined with a precision thickness gage (Hanatek FT3, UK). The mechanical properties of the MFC samples were measured with a Zwick D0724587 (ZwickRoell, Switzerland) universal testing device applying a strain rate of 4 mm/min and a gage length of 40 mm from strips having a width of 6 mm.

The assessed mechanical properties included tensile strength, which measures the maximum stress a specimen can withstand under uniaxial stress without breaking; tensile stiffness, determined as the slope of the stress–strain curve in the elastic region; toughness, which represents the deformation energy during tensile testing and is quantified as the area under the stress–strain curve; and strain, which measures the deformation under tensile stress and indicates how much the film elongates before breaking.

### Optical and scanning electron microscopy (SEM)

The amount of larger cellulose fibers or fiber wall residues left in the MFC samples in pilot grinding was visually evaluated from free-standing MFC films with a calculated grammage of 8 g/m$^2$. The films were made by casting 0.2% MFC suspension onto polystyrene Petri dishes. The suspensions were then left to dry overnight on a heated surface set at approximately 35 °C. After drying, the films were imaged under polarized light using a Leica Leitz Laborlux D (Germany) optical microscope.

The microstructure of the MFC obtained from pilot grinding was illustrated using SEM imaging with a Zeiss UltraPlus device (Germany). The sample was visually diluted to a very low concentration and dispersed using an IKA Yellowline DI 25 Basic homogenizer at 9 500 rpm for 1 min. It was then pipetted directly onto an aluminum SEM specimen stub. A secondary electron detector was used for the SEM images to maximize topographical contrast, with magnifications of 10 000 × and 50 000x. The true magnification for each image is indicated by the scale bars in Fig. 3. The samples were sputter-coated with a platinum/palladium coating of a few nanometers in thickness using a Leica EM ACE600 sputter coater before imaging. The particle width was analyzed using ImageJ software (version 1.54i), developed by Wayne Rasband and contributors at the National Institutes of Health, USA.

## Results

### Microscopy imaging of MFC from pilot grinding

Optical and electron microscopes were used to visualize the morphology and dimensions of the MFC. Figure 2 illustrates the progress of microfibrillation for each set of disc geometries used in pilot grinding after the final four passes (from the 3rd to 6th pass). As can be seen, after the third and the fourth pass, a lot of fibers and fiber fragments are still visible, but their amount decreases clearly after the fifth and especially after the sixth pass, and the samples

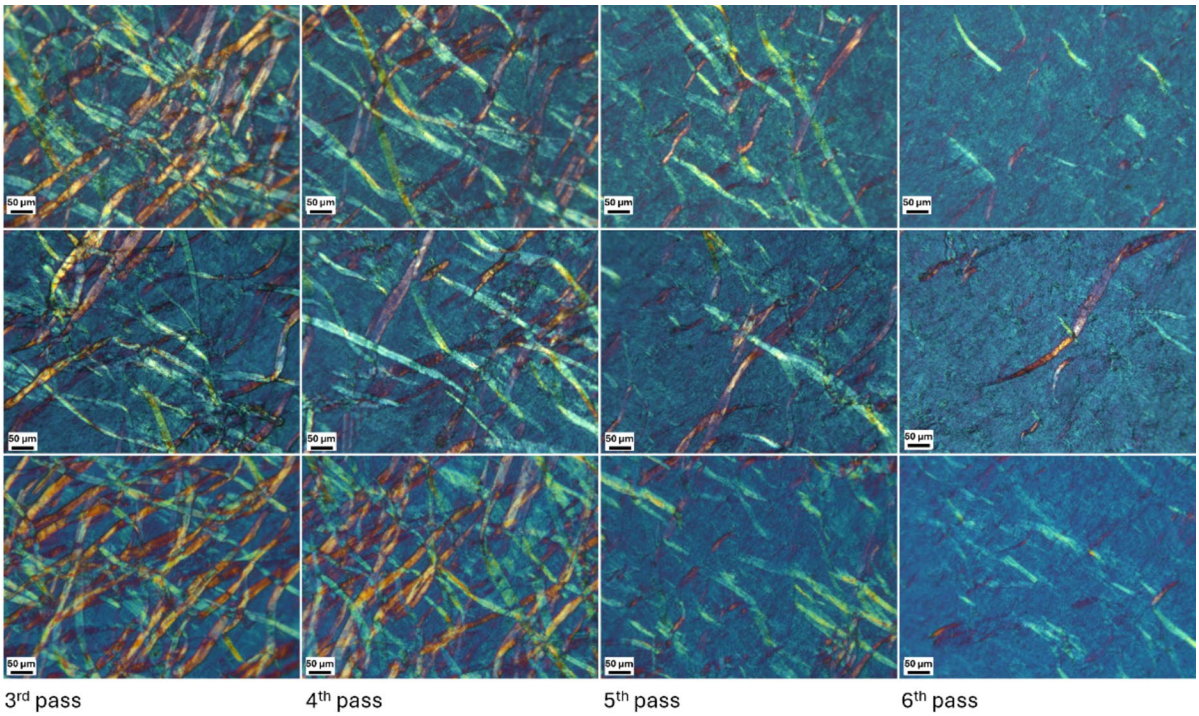


**Fig. 2** Progress of microfibrillation in pilot grinding from 3rd to 6th pass as imaged with a polarized light microscope. First row: Pilot1 Fine disc, second row: Pilot2 Coarse disc, third row: Pilot3 Fine disc with modified inlet

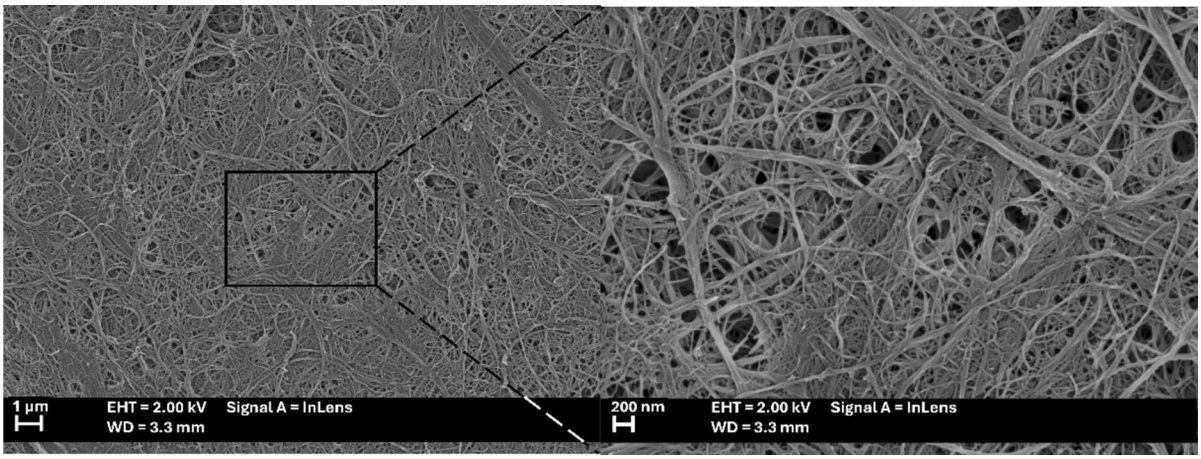


**Fig. 3** SEM images of MFC of test series Pilot1 after the 6th grinding pass

have a more homogeneous appearance. However, the residual larger fragments are still visible also after the sixth pass. However, the residual larger fragments are still visible also after the sixth pass.

The quality of MFC after the sixth pass of pilot grinding can be examined more closely in Fig. 3, which displays SEM images of the prepared sample from the Pilot1 test series. The sample consisted of

individualized elongated and slender nanofibrils, but there were also larger fibrils and fibril agglomerates present. The obtained nanofibrils have a length of several micrometers (Fig. 3, left) and their width seem to be mostly below 200 nm (Fig. 3, right). The average width was determined to be 75 nm, with a median of 55 nm, based on analysis of 400 particles.

## Energy consumption vs. size reduction based on equivalent diameter

Figure 4 shows that the experimental pilot grinding data on specific energy consumption and the change in the apparent specific surface area, which is directly proportional to $\Delta D^{-1}$, fits power-law curves excellently and the value of the exponents is close to 1 (ranging from 0.99 to 1.098), indicating that the microfibrillation closely follows Rittinger's law for fine grinding. The coefficient related to K in Eq. 5 varied due to differences in disc patterns. In pilot grinding, the range of the coefficient was between 0.052 and 0.079. Each test series can be considered replicates with respect to uncertainty in the experimental and analytical procedures. Therefore, the uncertainty of the slopes can be evaluated by calculating a confidence interval (*CI*) using the equation:

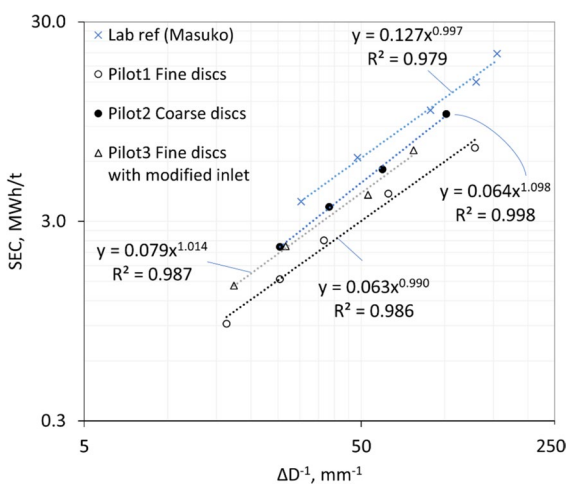


**Fig. 4** Specific energy consumption of microfibrillation as a function of change in inverse equivalent diameter (directly proportional to SSA) of MFC

$$CI = b \pm z\frac{\sigma}{\sqrt{n}} \tag{7}$$

where b is the average of the exponents,

$z$ is a critical value from the standard t-distribution table,

$\sigma$ is the standard deviation of the exponents, and.

$n$ is the number of samples.

For a two-tailed t-test with 2 degrees of freedom and a 95% confidence level, the CI is calculated as:

$$CI = 1.034 \pm 4.303\frac{0.0567}{\sqrt{3}} = 1.034 \pm 0.141 \tag{8}$$

The variability in the exponent values is small, and with 95% confidence, the exponent falls between 0.89 and 1.18. Thus, it can be said with high confidence that the microfibrillation data is consistent with Rittinger's law.

Also, the microfibrillation with the lab-scale Masuko grinder adhered to Rittinger's law (exponent 0.997), when the generation of a new surface was large enough. The coefficient (K = 0.127) was greater than in the pilot experiments, which can be explained by a combination of lower grinding consistency and the geometrical differences of the grinders and discs. Furthermore, in Masuko grinding, the feed consisted of intact birch pulp fibers, whereas in pilot grinding, pre-refined cut fibers were used. The agreement between the pilot and lab grinding results suggests that no significant systematic error was present in the pilot grinding tests.

## Generation of nanofibers

The content of nanofibers by the centrifugation method was measured from the samples of the last two stages in each pilot grinding series; they are presented in Fig. 5. The nanosized material content increased exponentially with a decreasing equivalent diameter of the microfibrillated cellulose. Therefore, it is evident that the accuracy of image analysis measurement was reduced as microfibrillation progressed, because the number of optically visible particles decreased. However, in pilot grinding the content remained relatively low, less than 12%, even at higher specific energy consumptions.

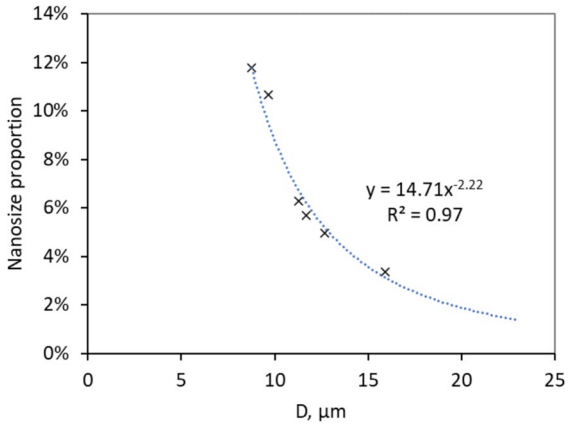


**Fig. 5** Content of nanosized particles as a function of equivalent diameter of the MFC samples from pilot grinding (finalfia two stages of each series)

## Apparent specific surface area vs. mechanical properties of MFC nanofilms

The apparent specific surface area here refers to the inverse of the equivalent particle diameter, without the coefficient of $6/\rho$ (see Eq. 4), which was assumed to be a constant.

The tensile strength of the nanofilms developed quite rapidly near its maximum level of about 200 MPa as the SSA increased, after which the strength remained practically unchanged, although the SSA increased significantly as grinding progressed (Fig. 6a). In pilot grinding, the disc pattern did not affect the maximum level of tensile strength, but with coarser disc patterns, a larger SSA, i.e., a smaller particle size, was required for the same tensile strength level. Laboratory grinding did not differ from pilot grinding, even though it reached slightly higher maximum tensile strengths, around 220 MPa. The tensile stiffness developed similarly to the tensile strength as grinding progressed and the SSA increased (Fig. 6b). With pilot grinding, a tensile stiffness level of about 9 GPa was achieved although a maximum of 10.9 GPa was recorded with the fine disc pattern. With Masuko grinding, a level of 11.5 GPa was reached.

Pilot grinding produced MFC with favorable elongation properties, which were also reflected in its toughness (Figs. 6c and 6d). Toughness increased almost linearly with increasing SSA, i.e., increasing $D^{-1}$ up to 100 $mm^{-1}$, especially when the fine disc pattern (i.e., in Pilot1 and Pilot3) was used. However, the extended grinding resulted in a point of "overgrinding" (Pilot1 series) where toughness and the strain at break dropped by about 25% in the final pass. This could be a consequence of too harsh grinding conditions which might have caused defects and cuts in nanofibers and degradation of cellulose chains.

In lab grinding, no similar drop in toughness and strain was observed, although extended grinding of MFC in terms of SSA was applied. However, a clear turning point in the development of toughness could be seen. After a steep increase to a $D^{-1}$ of 65 $mm^{-1}$, toughness increased at a much slower rate. In this respect, the behavior resembled pilot grinding with the coarse disc pattern (Pilot2). For a toughness level of 14 $MJ/m^3$, more than 50% higher SSA was needed in lab grinding than in the pilot grinding with fine discs (Pilot3).

## Discussion

Size reduction undergoes several stages in microfibrillation as a function of the disintegration energy applied. First the fibers are fibrillated internally, causing the lamella structure to loosen, then the fibers are cut and split, and the lamella structure are peeled off, after which the nanofiber bundles begin to separate and finally elementary fibrils detach from the bundles. These stages are not clearly distinguishable, but they are interlapped during grinding. One might expect that the grinder design and grinding conditions would affect the grinding mechanisms but, as hypothesized, the generation of new specific surface area was mechanistically similar and the same comminution model, i.e., Rittingers' law, was applicable in each case studied here. Although the grinder and disc design did not affect the grinding mechanism, they did affect the level of energy needed for a given increase in specific surface area. In other words, constant K in Eq. (5) describes how effectively energy is applied for the disintegration of the fiber structure from macro level to micro and nano levels. This is affected by the grinder and grinder disc design as well as pulp properties, i.e., the inherent strength of fibers and their structural integrity alongside consistency.

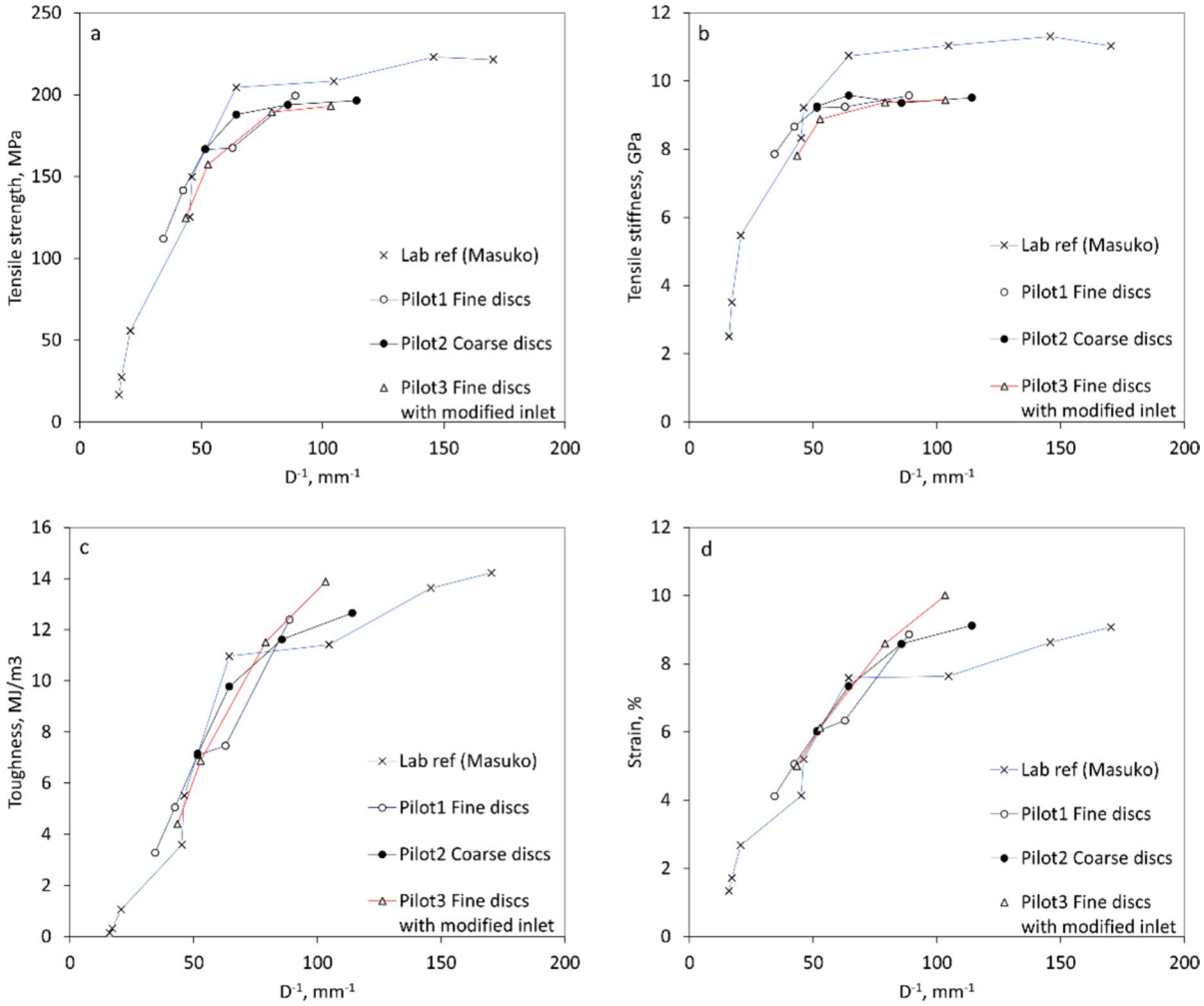


**Fig. 6** Development of the mechanical properties of MFC as a function of the inverse of equivalent diameter (directly proportional to SSA): **a** tensile strength, **b** tensile stiffness, **c** toughness, and **d** strain at break

## Apparent specific surface area as an indication of energy consumption

In both lab- and pilot-scale disc grinders, the energy consumption was found to adhere well to Rittinger's law of comminution when the equivalent sphere diameter calculated from the optical image analyzer data was used as the characteristic size, indicating that energy was consumed in the generation of new particle surfaces. This holds true when pulp is disintegrated into sufficiently small particles because the law is only valid in fine grinding. Thus, the energy needed for size reduction in microfibrillation can be predicted within a reasonably wide range using an optical fiber analyzer. This is possible because the amount of optically invisible sub-micron particles remains relatively low and also since their amount is related to visible particles. However, if a very fine size is targeted, the optical analyzer starts to underestimate size reduction due to its resolution limit.

Energy consumption for a given increase in the specific surface area is dependent not only on material properties including the size of the original fibers but also on grinder type and grinding conditions. Lab grinding with the Masuko grinder apparently consumed more energy for a given increase in SSA, but this was partly since grinding was started with intact cellulose fibers while, in the pilot experiments,

fibers were shortened by pre-refining. The lower consistency used in the Masuko grinder can theoretically explain 25% of the excess energy consumption in comparison to pilot grinding. However, consistency also affects pulp flowability and retention time between discs, and the combined effect may not be straightforward. The design of discs, geometrical dimensions of the grinders, and the texture of the surfaces were different, which affected mechanical energy transfer to the pulp suspension.

The apparent specific surface area of MFC particles determined by the equivalent diameter of spheres differs from the actual specific surface area. This discrepancy originates from the fact that microfibrillation loosens the fibrillar structure of cellulose fibers, generating or opening micro- and mesopores. Interestingly, the apparent and factual specific surface areas seem to be interrelated. This can be deduced from a prior study (Moser et al. 2016) where the actual specific surface area of bleached softwood sulfite pulp, measured by either krypton or xyloglucan adsorption, is presented as a function of the energy consumption of microfluidization. Excluding the highest energy consumptions, their data follow Rittinger's law precisely, as shown in Fig. 7, where exponents 1.01 and 1.02 for krypton (a) and xyloglucan (b) are recorded, respectively. The difference between the adsorption methods stems from the size difference between krypton and xyloglucan. Krypton, having an atom diameter of 0.4 nm, can penetrate micro and mesopores, whereas xyloglucan, with a molecular length of 640 ± 340 nm (Kozioł et al. 2015), cannot. Consequently, the latter may offer a better representation of the external surface area of particles that corresponds to the equivalent diameter based on image analysis used here. Furthermore, its predictive power to evaluate the relationship between energy and an increase of the specific surface area is wider than that of krypton adsorption. The increase in specific surface area measured with krypton virtually did not change after 12 MWh/t, whereas, with xyloglucan, a linear response to energy applied up to 27 MWh/t was observed.

## Apparent specific surface area as a characterization of MFC grade

Both lab- and pilot-scale grinding seemed to yield quite similar responses with respect to the development of MFC nanofilm strength properties relative to SSA. This outcome is somewhat unexpected because there are many dissimilarities between the grinders. For instance, the geometry of the discs and the texture of the disc surfaces are different.

Mechanical grinding of bleached birch kraft pulp yielded MFC with a good combination of strength properties. Tensile strength and stiffness reached their near maximum values with relative low energy consumption and a modest increase in SSA, while toughness consistently increased with increasing SSA up to a point that could be considered the grinding limit, after which the mechanical properties started to deteriorate. In pilot grinding with a fine disc pattern, a tensile strength of 199 MPa, tensile stiffness of 9.6 GPa, and toughness of 12.4 MJ/m$^3$ were recorded while applying a specific energy of only 4.1 MWh/t, corresponding to an SSA of about 90 mm$^{-1}$. In contrast, in lab-scale Masuko grinding, similar strength properties were obtained, with values of 205 MPa, 10.9 GPa, and 11.2 MJ/m$^3$, respectively, when interpolated to the same SSA. However, energy consumption was twofold higher, at 8.5 MWh/t. These high

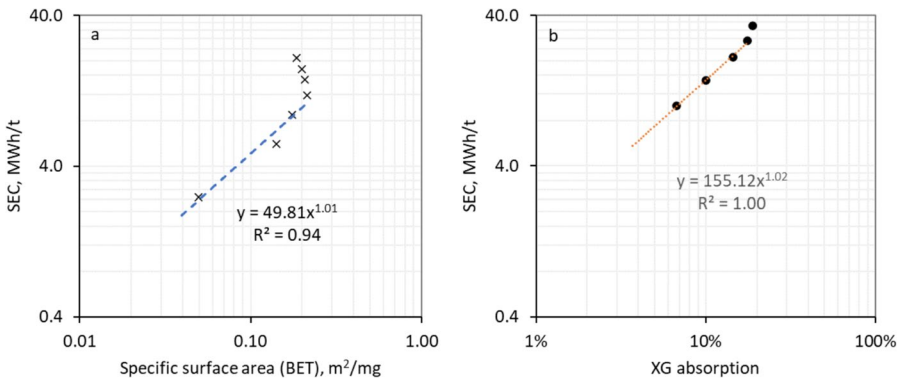


**Fig. 7** Increase in the specific energy consumption during softwood pulp microfibrillation with a microfluidizer, plotted against the specific surface area measured by (**a**) krypton gas (BET) and (**b**) xyloglucan (XG) adsorption. Chart adapted from data presented in (Moser et al. 2016)

mechanical strength values indicate that the MFC had high aspect ratios and hydrogen bonding degrees (Mokhena et al. 2021).

The increase in specific surface area observed at the beginning of grinding appeared to correlate with tensile strength and stiffness. However, with further grinding, there was only a little change in strength and stiffness despite a significant increase in specific surface area. In other words, the tensile strength and stiffness of MFC films may not necessarily be reliable indicators for assessing the grade of MFC. On the other hand, the development of toughness during grinding consistently aligns with the increase in specific surface area, making it a better measure of MFC grade.

### Monitoring of microfibrillation with an optical fiber analyzer

Commercial MFC production must fulfill given specifications, which means that manufacturing processes need to be controllable and monitorable, preferably based on online measurements. Although this study employed a laboratory fiber image analyzer, the methodology chosen is suitable for online measurement as well. For example, the method does not need fine adjustment of sample consistency, but dilution is done automatically by the device itself based on the optical concentration of visible particles in the samples. The measurement is also statistically reliable since the calculation of dimensions is based on millions or even tens of millions of MFC particles. Thus, the accuracy of the measurement appeared to be excellent with the coefficient of variation for the equivalent diameter and SSA being less than 2% for well-dispersed samples.

The progress of microfibrillation, in respect of particle size reduction and corresponding development of the mechanical properties of MFC nanofilms, could unexpectedly be successfully monitored with the optical fiber analyzer long before the resolution of the measurement became an obstacle. The limiting factor in measurements based on image analysis is the wavelength of light, which theoretically restricts the size of particles that can be observed. However, the results suggest that optically measured particle size reflects changes in the overall particle size distribution.

Another issue is related to the settings of the analyzer when adjusting the sample consistency to ensure an adequate number of visible particles in the images. As grinding progresses and the number of visible particles decreases, the device tends to increase the sample consistency. Consequently, particles that were optically invisible begin to contribute to the opacity of the images, thereby reducing resolution. Additionally, particle flocculation and overlapping may occur. However, the operating mode of the analyzer could potentially be programmatically adjusted to circumvent these issues. The analyzer is not fully optimized for MFC as far as we know.

The fraction of optically invisible particles is unknown, but it may correlate to the content of nanosized fibers measured by centrifugation. As shown here, the amount of invisible particles affects the parameters in the Rittinger equation and the relationship between particle size reduction and specific energy consumption. Although the optical fiber analyzer is widely applicable for current industrially relevant MFC production, the development of the fiber analyzer might be directed to the analyzing of particles below the resolution limit of the optical method. One approach could be to use the near infrared (NIR) electromagnetic spectrum which lies above that of visible light, from 700 to 2500 nm. As shown by (Osong et al. 2016), NIR responds to the volume of nanosized particles in homogenized TEMPO mediated pulp suspensions.

## Conclusions

Rittinger's law of comminution provides a theoretical foundation for understanding the microfibrillation of kraft pulp with disc grinders. This study demonstrates that the relationship between the apparent specific surface area in terms of equivalent diameter derived from the length and width of MFC particles and energy consumption is measurable over an industrially relevant range using a state-of-the-art optical fiber analyzer. The apparent specific surface area predicts the progress of microfibrillation and the development of strength properties of MFC, especially regarding the toughness of MFC films. The optical fiber image analyzer is ready for online operation and has the potential to be applied in the optimization,

monitoring, and control of mechanical MFC production processes.

**Acknowledgments** We would like to thank Jani Österlund, Elisa Wirkkala, and Maija Järventausta for their contribution to the experiments and laboratory analyses. This research work used the facilities of Tampere Microscopy Center, Tampere, Finland.

**Author contributions** A.Ä.: conceptualization, methodology, data analysis, original draft J.S., H.L.: writing—review & editing; O.L.: planning and conducting of lab grinding experiments, writing—review & editing O.E., S.S., and T.B.: planning and conducting of pilot grinding experiments and microscopy images of pilot MFC, writing—review & editing.

**Funding** Open Access funding provided by University of Oulu (including Oulu University Hospital). The research was conducted as part of the Sustainable Binders and Coatings (SUSBINCO) project (No. 2447/31/2021), funded by the Bio&Circular Finland program of Business Finland, and the Green Adaptable Method for Refining Lignocellulosic Materials to High-value Components (GRAM) project (No. 10894/31/2022), funded by the ExpandFibre program of Business Finland.

**Data availability** Data used in this study is available upon request.

**Declarations**

**Conflict of interest** The authors declare that they have no competing financial interests or personal relationships that could have influenced this work**.**

**Consent for publication** All authors have agreed to publish this research.



## References

Amini E, Hafez I, Tajvidi M, Bousfield DW (2020) Cellulose and lignocellulose nanofibril suspensions and films: a comparison. Carbohyd Polym 250:117011. https://doi.org/10.1016/j.carbpol.2020.117011

Ämmälä A, Sirviö JA, Liimatainen H (2022) Pine sawdust modification using Fenton oxidation for enhanced production of high-yield lignin-containing microfibrillated cellulose. Ind Crop and Prod 186:115196. https://doi.org/10.1016/j.indcrop.2022.115196

Balea A, Fuente E, Monte MC et al (2020) Industrial application of nanocelluloses in papermaking: a review of challenges, technical solutions, and market perspectives. Molecules 25:526. https://doi.org/10.3390/molecules25030526

Balea A, Fuente E, Tarrés Q et al (2021) Influence of pretreatment and mechanical nanofibrillation energy on properties of nanofibers from aspen cellulose. Cellulose 28:9187–9206. https://doi.org/10.1007/s10570-021-04109-w

Dias OAT, Konar S, Leão AL et al (2020) Current state of applications of nanocellulose in flexible energy and electronic devices. Front Chem 8:420. https://doi.org/10.3389/fchem.2020.00420

Felgueiras C, Azoia NG, Gonçalves C et al (2021) Trends on the cellulose-based textiles: raw materials and technologies. Front Bioeng Biotechnol 9:608826. https://doi.org/10.3389/fbioe.2021.608826

Foster EJ, Moon RJ, Agarwal UP et al (2018) Current characterization methods for cellulose nanomaterials. Chem Soc Rev 47:2609–2679. https://doi.org/10.1039/C6CS00895J

Heise K, Kontturi E, Allahverdiyeva Y et al (2021) Nanocellulose: Recent fundamental advances and emerging biological and biomimicking applications. Adv Mater 33:2004349. https://doi.org/10.1002/adma.202004349

Hukki RT (1961) Proposal for a solomonic settlement between the theories of von Rittinger, kick and bond. Trans AIME 220:403–408

Jennings B, Parslow K (1988) Particle size measurement: the equivalent spherical diameter. Proc R Soc Lond A 419:137–149. https://doi.org/10.1098/rspa.1988.0100

Kangas H, Lahtinen P, Sneck A et al (2014) Characterization of fibrillated celluloses. A short review and evaluation of characteristics with a combination of methods. Nord Pulp Pap Res J 29:129–143. https://doi.org/10.3183/npprj-2014-29-01-p129-143

Kelly PV, Gardner DJ, Gramlich WM (2021) Optimizing lignocellulosic nanofibril dimensions and morphology by mechanical refining for enhanced adhesion. Carbohyd Polym 273:118566. https://doi.org/10.1016/j.carbpol.2021.118566

Kozioł A, Cybulska J, Pieczywek PM, Zdunek A (2015) Evaluation of structure and assembly of xyloglucan from tamarind seed (*Tamarindus indica* L.) with atomic force microscopy. Food Biophys 10:396–402. https://doi.org/10.1007/s11483-015-9395-2

Kumar V, Bollström R, Yang A et al (2014) Comparison of nano- and microfibrillated cellulose films. Cellulose 21:3443–3456. https://doi.org/10.1007/s10570-014-0357-5

Laitinen O, Suopajärvi T, Liimatainen H (2020) Enhancing packaging board properties using micro- and nanofibers prepared from recycled board. Cellulose 27:7215–7225. https://doi.org/10.1007/s10570-020-03264-w

Miao C, Hamad WY (2013) Cellulose reinforced polymer composites and nanocomposites: a critical review. Cellulose 20:2221–2262. https://doi.org/10.1007/s10570-013-0007-3

Miller J (2022) Cellulose nanomaterials production summary. In: TAPPI International nanotechnology division. https://www.tappinano.org/for-producers/production-summary/. Accessed 24 May 2024

Mokhena TC, Sadiku ER, Mochane MJ et al (2021) Mechanical properties of cellulose nanofibril papers and their bionanocomposites: a review. Carbohyd Polym 273:118507. https://doi.org/10.1016/j.carbpol.2021.118507

Moser C, Henriksson G, Lindström ME (2016) Specific surface area increase during cellulose nanofiber manufacturing related to energy input. BioResources. https://doi.org/10.15376/biores.11.3.7124-7132

Nair SS, Zhu JY, Deng Y, Ragauskas AJ (2014) Characterization of cellulose nanofibrillation by micro grinding. J Nanopart Res 16:2349. https://doi.org/10.1007/s11051-014-2349-7

Osong SH, Norgren S, Engstrand P et al (2016) Qualitative evaluation of microfibrillated cellulose using the crill method and some aspects of microscopy. Cellulose 23:3611–3624. https://doi.org/10.1007/s10570-016-1068-x

Pennells J, Heuberger B, Chaléat C, Martin DJ (2022) Assessing cellulose micro/nanofibre morphology using a high throughput fibre analysis device to predict nanopaper performance. Cellulose 29:2599–2616. https://doi.org/10.1007/s10570-021-04405-5

Perumal AB, Nambiar RB, Moses JA, Anandharamakrishnan C (2022) Nanocellulose: recent trends and applications in the food industry. Food Hydrocoll 127:107484. https://doi.org/10.1016/j.foodhyd.2022.107484

Serra-Parareda F, Aguado R, Tarrés Q et al (2021) Chemical-free production of lignocellulosic micro- and nanofibers from high-yield pulps: synergies, performance, and feasibility. J Clean Prod 313:127914. https://doi.org/10.1016/j.jclepro.2021.127914

Varanasi S, He R, Batchelor W (2013) Estimation of cellulose nanofibre aspect ratio from measurements of fibre suspension gel point. Cellulose 20:1885–1896. https://doi.org/10.1007/s10570-013-9972-9

Wills BA, Napier-Munn T (2015) Wills' mineral processing technology: an introduction to the practical aspects of ore treatment and mineral recovery. Butterworth-Heinemann, Oxford

Zambrano F, Starkey H, Wang Y et al (2020) (2020) Using micro- and nanofibrillated cellulose as a means to reduce weight of paper products: a review. BioResources 15(2):4553–4590

Zhang X, Kitin P, Agarwal UP et al (2023) Characterizing lignin-containing microfibrillated cellulose based on water interactions, fibril properties, and imaging. Carbohyd Polym 316:120996. https://doi.org/10.1016/j.carbpol.2023.120996